2011 IEEE/RSJ International Conference on
Intelligent Robots and Systems
September 25-30, 2011. San Francisco, CA, USA

# Translational Damping on Flapping Cicada Wings

Perry Parks, Bo Cheng, Zheng Hu, and Xinyan Deng, *Member, IEEE*

***Abstract*—We measured the dynamic damping of a pair of flapping cicada wings mounted on a robotic insect thorax mechanism capable of high frequency flapping. The damping coefficients were derived based on the measurements of the wing-thorax mechanism translating along its body principal axes. The robotic mechanism has a 10cm wingtip-to-wingtip span, flaps up to 65Hz, and weigh 2.86 gram including the motor and wings. To measure the flapping induced damping during translation, we developed a pendulum system mounted with encoder, and attached the flapper at the end and in different orientations such that its motion is along its principle axes. The damping of the flapper is then calculated from the decaying rate of the magnitude of the oscillating pendulum. The damping coefficients calculated from the experiments are very close to those estimated based on our mathematic models using Blade-Element Theory (BET) and quasi-steady aerodynamic models. As expected, the damping linearly increases with the flapping frequency and is most prominent along forward/backward direction.**

## I. Introduction

Insects and other flapping-wing fliers can subtly change their wing kinematics to achieve fast maneuvers. It has been found that during fast maneuvers, there exists significant aerodynamic damping resulted from flapping wings. For example, during fast yaw turns (or saccade), a strong damping torque is produced not only to help slow down the turns during deceleration, but also help to provide passive stability to the flier [1]. It was also found that, during pitch maneuvers of a hawk moth, the changes of wing kinematics are strongly related to the pitch rate rather than the pitch acceleration. In other words, significant efforts are made by the insect to overcome the velocity-dependent damping during the maneuvers.

Understanding the damping characteristics of flapping wings is not only important for studying the flight behavior of animals but also for designing future flapping-wing Micro Air Vehicles (MAVs). It is not only critical in modeling and analyzing the flight dynamics of flapping flight, but also in flight control. For example, the understanding of how much damping is experienced when the robot is translating or rotating in the air helps to determine the amount of wing kinematic changes that can achieve certain flight performance.

Recently, understanding the effect of body movements on the flight dynamics (changes of resultant aerodynamic forces and torques) is of particular interests and several studies have addressed this subject [2-9]. However, the analysis and experiments on life-scale flapping-wing device in a realistic operating condition (such as high frequency flapping in the air) is still lacking, although some experiments have been performed on dynamically scaled robotic wings in an oil tank [3] where inertia forces, wing flexibility, and fluid structural interactions resulted from real flying conditions in air are neglected. In this study, we extend our analysis and experiments by using a 2.86g robotic insect flapper flapping up to 65Hz in air [10], and a custom-designed pendulum system, to measure the damping generated by the life-sized robot when it is translating along its body principal axes. These measurements are then compared to the theoretical predictions.

This work was supported in part by NSF Grant CMMI-1100764 to X Deng.
The School of Mechanical Engineering, Purdue University, West Lafayette, IN 47906. Email: xdeng@purdue.edu

## II. Experiment Design & Procedure

### A. Robotic Insect Prototype

We developed an insect-size flapping mechanism, shown in Fig.1. It employs horizontal stroke plane similar to most of Dipteral insects. Here we employ a passive wing rotation mechanism where the pronation and supination of wings results from the inertia and aerodynamics forces during the wing reversal. Mechanical stoppers were employed at the stroke reversal and the angle of attack (AOA) for upstroke and downstroke is $45^o$ during midstroke. The wing stroke angle amplitude is $130^o$; a frequency of 65Hz was achieved at 12V power supply; the device has 10cm wingtip-to-wingtip span and the height is 28mm; the total weight is 2.86 gram (including the motor); the weight for a man-made wing is 0.04gram and a dried cicada wing 0.02gram, see Figure 2.

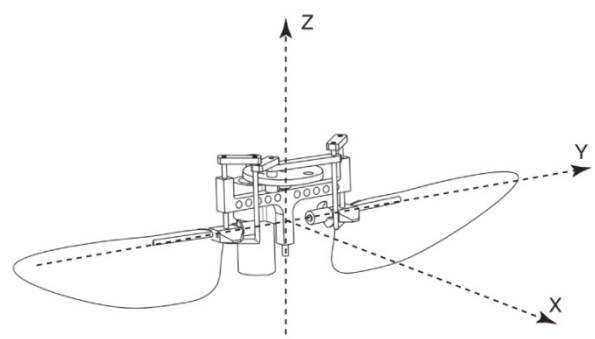


Fig, 1. A schematic of the robotic insect and its coordinate system.

The motion of wings were videotaped by a high speed camera and the wing kinematics was obtained from the camera images as shown in Figure 3. The flapping frequency vs. input voltage are shown in Figure 4(a). We tested both man-made wings and cicada wings, and found comparable aerodynamic performances between the two up to 40Hz. Figure 4(b) shows the lift force generated at different flapping frequency. For this study, we limit the flapping frequency to

be up to 40Hz to avoid nonlinearity and aerodynamic force saturation, as observed on the man-made wings in Figure 4(b). In fact, in nature cicada beat their wings at 30-40Hz, which seems to be optimal for their wings. Frequencies higher than 60Hz tend to either damage their wing roots or cause wing surface buckling, as we found in our experiments.

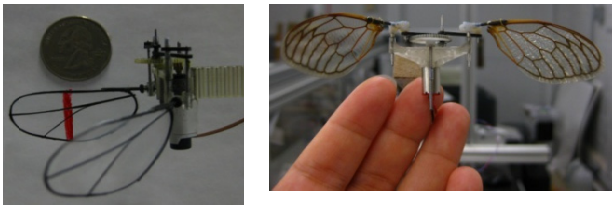

Fig 2. Man-made (left) and cicada (right) wings mounted on the high frequency robotic thorax mechanism.

## B. Experiment Design

The experiment needs to be able to quantify the damping characteristics of the robotic insect prototype for different translational axes and a range of wingbeat frequencies. For this work, we used the cicada wings whose results are representative, since our man-made wings have similar aerodynamic performance.

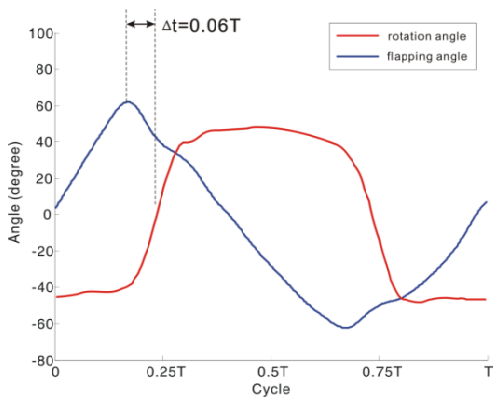


Fig 3. wing kinematics (flapping and rotation angles).

Because the magnitude of the damping is relatively small compared to that of total force, it is difficult to measure it directly using conventional force sensors. Therefore, we used a indirect method. The experiment described here employs a oscillating pendulum to provide translation along its peripheral for the robot mechanism attached at the end. The pendulum and the prototype are raised and then dropped from an initial angle and subsequent oscillation decay of the pendulum angle magnitude is recorded. Experiments are performed by allowing the prototype to operate at different wingbeat frequencies (including zero wingbeat frequency, i. e. non-flapping). The recorded oscillation datasets can then be processed to determine the change in magnitude decay rate, which will be used then to determine the damping coefficients. The same procedure can be used for different orientations of the prototype so that damping coefficients along its principle axes are quantified.

## C. Pendulum Apparatus Design

The experimental apparatus consists of a pendulum mounted on a horizontal shaft suspended by two bearings (Figure 5). The bearings fit in a bracket which is screwed to a stationary frame. Perpendicular fixture of the pendulum rod to the horizontal shaft is achieved using a machined joining block and set screws. The robotic insect prototype is attached to the end of the pendulum and wired to a voltage source in order to power the onboard DC motor (The wiring doesn't interfere with the pendulum). The plastic mount used to attach the prototype to the end of the pendulum is designed such that the prototype may be positioned in different orientations; this allows the experiment to be carried out for three orientations: "forward-backward" (x axis), "left-right" (y axis) and "up-down" (z axis). Fig. 5 also illustrates the definitions of these three orientations.

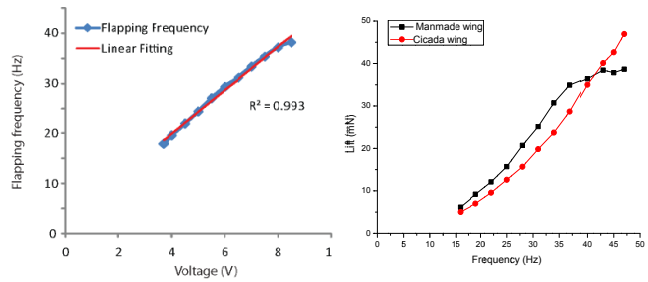


Fig 4. (left) Flapping Frequency at different input voltages; (right) Lift force generation at differnet flapping frequencies of man-made(black) and cicada (red) wings.

The apparatus allows the pendulum to oscillate freely after being lifted and released from an initial angle from the equilibrium. The voltage to the prototype's motor supplied by the voltage source may be altered between each experiment run to change the wingbeat frequency.

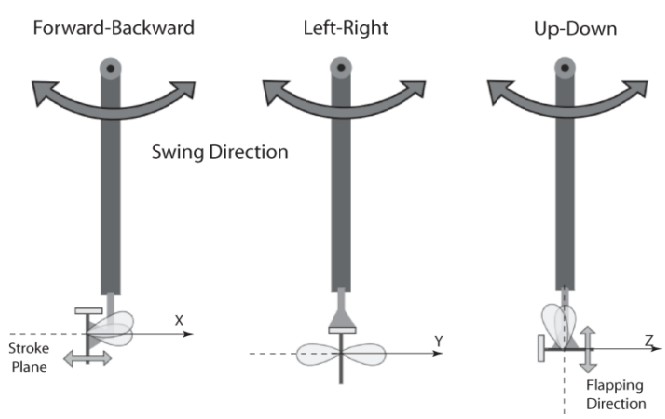


Fig. 5. An illustration of the three prototype orientations employed in this experiment. The dark rod is the pendulum, and the point at the top its center of rotation. Dotted lines indicate the stroke plane of the flapper.

A rotary encoder is mounted to the bracket and joined with the horizontal shaft so that it may measure the rotation angle of the pendulum. The encoder is in turn connected to an Arduino Duemilanove microcontroller (Smart Projects, Italy) which records the measurements. Table 1 lists the main components of the apparatus along with dimensions, where

applicable.

TABLE 1
APPARATUS COMPONENTS

| Component | Material | L/W/H[a] | Diameter[a] |
|---|---|---|---|
| Pendulum Rod | Aluminum | 37.94 / - / - | 0.96 |
| Shaft | Steel | 6.67 / - / - | 1.0 |
| Joining Block | Aluminum | 2.5 / 1.9 / 5.0 | - |
| Bearings (2X) | Steel | - | - |
| Bracket | Plastic | | |
| Shaft Coupling | Plastic | - | |
| Encoder | - | | |
| Arduino Duemilanove | - | - | - |

[a]Units in cm.

### D. Experiment Procedure

The procedure for performing the experiment for the "forward-backward" prototype orientation is described here, and the procedure for the other two orientations are similar. The robot prototype was first mounted to the end of the pendulum so that it will be moving as if in forward-backward flight while the pendulum swings (We consider the effect of rotational velocity at mounting position is negligible). Next the voltage source is set to the appropriate level. For the first run it is set to 0 volts for no flapping. Then the Arduino program is started so that it begins reading angular measurements from the encoder. The program waits until the user has raised the pendulum and begins recording measurements once the user drops the pendulum and the measurement falls below 300 units of resolution (~40 degrees). The Arduino then records the decaying waveform until the oscillation stops. When the oscillation stops the user saves the data and can start again with the voltage source set to 0.6 volts, increasing by 0.1 volt for each experiment until reaching 2.6 volts (a wingbeat frequency of about 34 Hz). The user performs a total of 22 experiments per orientation of the robot prototype.

## III. DATA PROCESSING AND ANALYSIS

### A. Principles for Data Processing

A pendulum is a nonlinear vibratory system, and therefore the standard methods for determining the damping ratio of a linear system (e.g. the "Log Decrement Method") do not apply. Here, we plot the experimental output and, using the same initial condition on the pendulum angle, simulate the second-order nonlinear pendulum model using MATLAB's ordinary differential equation (ODE) solving capabilities. Having determined the system inertia and center of mass, the only unknown is the damping coefficient(s).

After performing some trial ODE simulations on the datasets, it became apparent that a velocity-dependent damping model was not sufficient to describe the system. For this system, the following model which includes both velocity-dependent and Coulomb damping was used for the ODE simulation:

$$\ddot{\theta} = -\mathrm{mg} \times \frac{L_0}{I} \sin\theta - c_0 \times \frac{sgn(\dot{\theta})}{I} - \frac{c_1}{I}\dot{\theta} \qquad (1)$$

where $L_0$ *is* the length between pendulum joint and its center of gravity, $I$ is the pendulum moment of inertia with respect to the horizontal shaft's axis of rotation, $\theta$ and $\dot{\theta}$ are angle and velocity of the pendulum, $m$ is system mass, and *sgn()* represents signum function. The coefficients $c_0$ and $c_1$ are the coefficients of Coulomb and velocity-dependent damping, respectively. It should be noted here, the coulomb damping $c_0$ is resulted from the friction in the system joint; and the velocity-dependent damping $c_1$ is resulted from both the friction in the system joint and the damping generated by flapping wings. As will see later, the damping resulted from flapping wings can be calculated by subtracting the damping when there is no wing flapping.

### B. Data Processing Procedure

Since there is a delay between the time when the user releases the pendulum and the time when the Arduino begins recording angle measurements, the initial angle in the recorded data is not a constant. Consequently, the first data points are not at a position of zero initial velocity either. To address this, and to determine the initial angle condition needed for each simulation, the first data points of each dataset are removed such that each dataset then begins with zero initial velocity (pendulum at its highest position of a cycle). The initial angles are recorded for input as initial conditions to the simulation.

Each experiment dataset has corresponding $c_0$ and $c_1$ coefficients to characterize its damping. The method used to determine the values of these coefficients is to create an evenly-spaced sample grid of $c_0$ and $c_1$ values and then perform MATLAB simulations for each point on that space. The pair of coefficient values that result in a simulation plot most similar to the experiment plot are the ones chosen as the solution.

It is important to note that the period of oscillation in the experiment was observed to increase slightly with time. This is possibly due to the nonlinearities of the damping in the system. Because the damping model is assumed to be linear (except the Coulomb damping), it is impossible to duplicate the exact oscillation trajectory in the simulations. Instead, we choose to match the magnitude (i.e. the envelope) of oscillation, and consider the phase difference as error caused by the neglected nonlinearities. An example dataset illustrating this characteristic can be found in Fig. 6.

Now the "exponential decay envelope" are used for comparing the simulation to the experiment results. One way to determine the "envelope function" for the experiment is to trace a curve along the maxima. In this way, a piecewise-linear function was created by linking each maximum. The oscillation frequency of the pendulum is high enough that this piecewise-linear model is a close approximation to the real envelope. In processing the data, this is implemented as a function that is polled for any given

time $t$ so that it returns the result of linear interpolation between two maxima. Thus, it can be used to evaluate the proximity of any point to its corresponding point on the envelope function.

To evaluate the closeness of fit for a simulation plot of a given $c_0$ and $c_1$ pair, the maxima are found for the experiment plot and for the simulation plot and compared. Variance is used to determine the best $c_0$ and $c_1$ for each experiment. If each simulation maximum occurs at a time $t_i$, then the "variance" is defined here as the sum of all squared deviations of the simulation maximum at $t_i$ from the corresponding value of the experiment envelope function at the same time $t_i$. The simulation resulting in the lowest variance gives the desired $c_0$ and $c_1$ solution. In solving for $c_0$ and $c_1$ a first solution iteration was done using a coarsely-spaced grid of coefficients, followed by a second iteration using a fine-resolution coefficient grid with the "coarse solutions" as the center point of the grid.

## IV. Experiment Results

A plot showing a typical simulation solution with experiment measurement and envelope function overlaid is shown in Fig 6. It can be seen that the closeness of fit with respect to oscillation magnitude is very good (the fits are equally good for experiments using different orientations). The example of Fig. 6 demonstrates the effectiveness of the solution method for determining the best $c_0$ and $c_1$ pair for a given experiment.

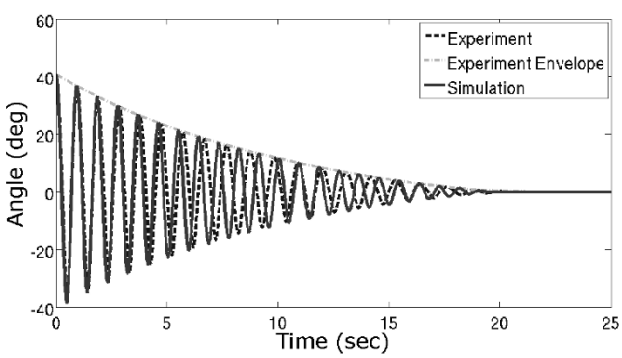


Fig. 6. The result of matching the model to the experiment measurement for a wingbeat frequency of 13.5 Hz. Resulting $c_0$: 0.0011; $c_1$: 0.00131. This result is the visualization of the simulation with $c_0$ and $c_1$ parameters which fit the experiment plot the most closely in terms of oscillation magnitude.

The results of the $c_0$ (Coulomb damping) for each orientation did not reveal any trend with respect to increasing wingbeat frequency. For each orientation the distribution of $c_0$ values was simply a scatter about a mean value. Thus, plots of $c_0$ versus wingbeat frequency are not shown here; instead, $c_0$ results will be simply stated in terms of a mean and standard deviation. For example, the mean value for the "up-down" orientation is the mean of all $c_0$ solutions (i.e. chosen solutions, not guesses) for each of the 22 experiment datasets in this orientation. The results for Coulomb damping are summarized in Table 2.

The velocity-dependent damping coefficient $c_1$ includes both the damping from system friction and from flapping wings. In order to identify the damping resulted from the flapping wings, each $c_1$ (for different flapping frequencies) is subtracted by an amount equal to the value of $c_1$ corresponding to 0 flapping frequency. Note that, when the wing is not flapping, the damping resulted from stationary wings is relatively small when compared to the one generated by flapping wings. For example, based on previously measured force coefficients for translating wings [11] we calculated that at 0.5 m/s translational velocity, the damping generated by non-flapping wings is at most about 9% (assuming the wing fully extended) of the one by flapping wings (assuming 30 Hz flapping frequency). We denote the $c_1$ after subtraction as $\tilde{c}_1$.

TABLE 2
Coulomb Damping $c_0$

| Prototype Orientation | Mean Value | Standard Deviation |
|---|---|---|
| "Up-down" | 1.0 | .18649 |
| "Forward-flight" | 1.1 | .14562 |
| "Left-right" | 1.1 | .15642 |

Mean and standard deviation of $c_0$ are in units of N*m*$10^{-3}$.

First, the results for the "forward-backward" orientation (travelling along X axis) is shown in Fig. 7.

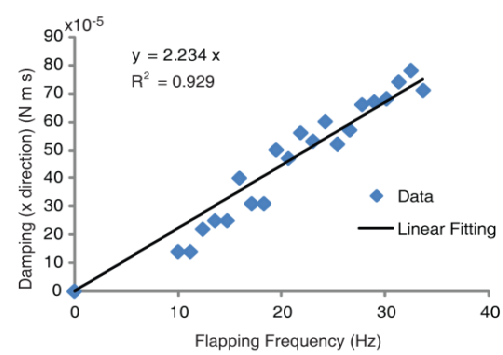


Fig. 7. Variation of velocity-dependent damping $\tilde{c}_1$ with wingbeat frequency for the "forward-backward" orientation.

The plot of velocity-dependent damping in Fig. 7 has a very clear trend demonstrating that the damping increases with wingbeat frequency. A linear fitting suggests that (also converted to the damping in terms of force, other than in terms of torque as in Eqn. 1),

$$F_x = (2.234/L^2)n\dot{\theta}L = (2.234/L^2)nv_x = 15.52nv_x, \quad (2)$$

where $F_x$ is the total force ( or damping, units : $10^{-5}$ Newton) along X direction, $v_x$ is the translational velocity along X axis and in this case equals to $\dot{\theta}L$, $L$ is the length of pendulum and n is wing flapping frequency. An estimation of the damping based on Blade-Element-Theory (BET) and quasi-steady aerodynamic model [12, 13] gives [3, 4]:

$$F_x = \rho S R \hat{r}_1^1(S) \Phi \overline{C_D(\alpha_0)\cos^2(\phi)\left|\frac{d\hat{\phi}}{d\hat{t}}\right|} n v_x = 17.12 n v_x, \quad (3)$$

where $\hat{r}_1^1(S)$ is the non-dimensional first moment of wing area, $\rho$ is fluid/air density, $S$ is wing area, $\phi$ is stroke angle, α is angle of attack, $\frac{d\hat{\phi}}{d\hat{t}}$ is the non-dimensional angular velocity of the wing and Φ and $n$ are wing-flapping amplitude and frequency. We can see that, the damping estimated based on BET is very close to the one calculated based on measured data.

Next, the results for the "left-right" orientation (travelling along Y axis) is shown in Fig. 8.

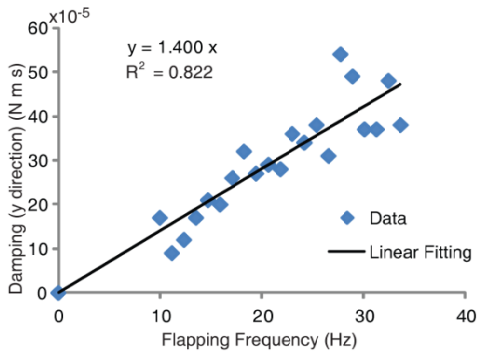


Fig 8. Variation of viscous damping $\tilde{c}_1$ with wingbeat frequency for the "left-right" orientation.

The $\tilde{c}_1$ plot shows a clear trend again: velocity-dependent damping increases with wingbeat frequency. In this "left-right" orientation the trend is quite clear, though there is more scatter than in the "forward-backward" orientation. A linear fitting suggests that,

$$F_y = (1.400/L^2) n \dot{\theta} L = (1.400/L^2) n v_y = 9.73 n v_y, \quad (4)$$

(units : $10^{-5}$ Newton) where $v_y$ is the translational velocity along Y axis. The estimation based on BET is [3]:

$$F_y = \rho S R \hat{r}_1^1(S) \Phi \overline{C_D(\alpha_0)\cos^2(\phi)\left|\frac{d\hat{\phi}}{d\hat{t}}\right|} n v_y = 9.00 n v_y. \quad (5)$$

Again, we can see that the measured value is very close to the BET estimation in this case. Note that, the damping in lateral direction is found to be smaller than the one in forward/backward direction (for both measurement and BET estimation).

Finally, the results for the "up-down" orientation (travelling along Z axis) is shown in Fig. 9.

The plot of $\tilde{c}_1$ for the "up-down" orientation in Fig. 9 appears to show a trend of increasing damping with wingbeat frequency. However, in this orientation, the trend is not nearly as clear as for the "forward-backward" orientation. For the sample of $\tilde{c}_1$ values having wingbeat frequencies between 10 Hz and 35 Hz, there appears to be a slight incline to the data points as the wingbeat frequency increases. It is important to note that the values of $\tilde{c}_1$ for the flapping cases are significantly higher than zero (non-flapping case). Thus, it is reasonable to say that a non-zero wingbeat frequency does affect the damping in the "up-down" orientation. The worse linear dependence on the flapping frequency in this case might due to the complex wing–wake interaction when the robotic insect is traveling into the wake below the stroke plane (i.e., traveling downward). A linear fitting gives:

$$F_z = (1.270/L^2) n \dot{\theta} L = (1.270/L^2) n v_y = 8.82 n v_z, \quad (6)$$

(units : $10^{-5}$ Newton) where $v_z$ is the translational velocity along Z axis. The estimation based on BET is (valid for both up and down translation) [3]:

$$F_z = 0.5 \rho S R \hat{r}_1^1(S) \Phi \overline{\frac{dC_L(\alpha_0)}{d\alpha}\left|\frac{d\hat{\phi}}{d\hat{t}}\right|} n v_z = 6.06 n v_z. \quad (7)$$

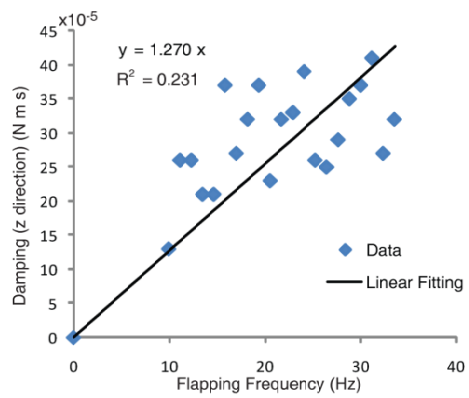


Fig. 9. Variation of velocity-dependent damping $\tilde{c}_1$ with wingbeat frequency for the "up-down" orientation. Clearly, increasing wingbeat frequency results in larger damping.

Compared to the first two cases, the BET seems to give the worst estimation of damping (about 30% lower than the measured value), but it still can be considered an acceptable estimation. The underestimation is possibly due to the wing-wake interaction, which may enhance the damping when traveling into the wake, but no conclusion can be made here and more detailed flow experiment and force measurement are needed to verify this hypothesis. In addition, it should be noted that, in this case, the damping is asymmetric when the pendulum is swinging from left to right and from right to left, because for the flapper, traveling upward and downward are aerodynamically different (not for left-right and forward-backward). Therefore, it may further complicate the damping measured in this case.

We can see that, for all three translating axes, the measured values are very close to the BET estimations. Therefore, significant damping resulted from flapping wings does exist on the robotic flapper tested. To see how it affects the flight, one can calculate that when flapping at 36Hz wingbeat frequency (generating enough lift to support 2.86g body weight) and traveling at 1m/s in forward/backward direction, the damping is about 20% of the body weight, which is corresponding to about 2 m/s$^2$ acceleration opposite to the direction of translation.

We see that it is not such a linear relationship as that of the "forward-backward" orientation (or possibly just not as inclined). It is also worth mentioning that the distribution of viscous damping values in the "up-down" orientation of Fig. 6 has a smaller span of values than the "forward-backward" viscous damping distribution of Fig. 4. A comparison of the span of viscous damping values for all three orientations studied is presented in Table 3.

Table 3 summarizes the span of $c_1$ values corresponding to each prototype orientation. The span of $c_1$ values serves as an indicator of the potential of wingbeat frequency to affect the viscous damping characteristics for the given orientation (i.e. the strength of the effect).

TABLE 3
VISCOUS DAMPING $C_1$ SPAN

| Prototype Orientation | Span of $c_1$ |
|---|---|
| "Forward-backward" | 7.8 |
| "Left-right" | 5.4 |
| "Up-down" | 4.1 |

Span of $c_1$ is in units of N*m*s*$10^{-4}$.

## V. CONCLUSION AND DISCUSSION

In this paper, experiments designed to measure the velocity-dependent damping resulted from flapping wings on a 2.86g robotic flapper are presented. It has been shown that the damping characteristics of the prototype robotic flapper are linked to the wingbeat frequency. The wingbeat frequency has been clearly shown to increase the damping substantially when the prototype is moving along its X (forward-backward), Y (left-right) and Z (up-down) axes. Strong linear dependence of damping on flapping frequency is found for "forward-backward" and "left-right" translations. The "up-down" translation is more complicated because wing-wake interaction is presented in this case, and the damping has less linear dependence on flapping frequency.

From the measured damping, which is close to the analytical estimations based on BET, we can see that the damping is most strong when the prototype is traveling along "forward-backward" direction. If we assume to flight forward, the stroke plane is tilted to a certain degree and a portion of lift force is used to create forward force, then it can be estimated that at least 10º of tilt is required for traveling at 1 m/s when flapping at 36 Hz. Similar estimation can be made when different control strategies are used (e.g., change of angle of attack and stroke amplitude), and the amount of changes of wing kinematics can be roughly estimated.

The effect of wingbeat frequency on Coulomb damping appears negligible. In fact, the mean values of Coulomb damping for each of the three orientations studied is essentially equal (Refer to Table 2). This result is understandable since the main source of Coulomb damping is likely the bearings of the pendulum mount. If this is assumed to be true, then the separation of the system damping into a Coulomb component and a viscous component (See Equation 1) is actually helpful since it allows us to conceptually separate the robot prototype from the experiment apparatus. Additionally, any lift force generated by the robot prototype by flapping will be small in magnitude compared with the existing normal force felt by the bearings from the pendulum rod. So one cannot expect a large change in Coulomb friction at the bearings.

## REFERENCES


[1] T. L. Hedrick, B. Cheng, and X. Deng, "Wingbeat Time and the Scaling of Passive Rotational Damping in Flapping Flight," *Science,* vol. 324, pp. 252-255, April 10 2009.

[2] A. J. Bergou, L. Ristroph, J. Guckenheimer, I. Cohen, and Z. J. Wang, "Fruit Flies Modulate Passive Wing Pitching to Generate In-Flight Turns," *Physical Review Letters,* vol. 104, p. 148101, 2010.

[3] B. Cheng and X. Deng, "Mathematical Modeling of Near-hover Insect Flight Dynamics," in *In ASME DSCC Dynamic Systems and Control Conference* Cambridge, Massachusetts, 2010.

[4] B. Cheng, S. Fry, Q. Huang, and X. Deng, "Aerodynamic damping during rapid flight maneuvers in the fruit fly Drosophila " *Journal of Experimental Biology,* vol. 213, pp. 602-612, 2009.

[5] B. Cheng, S. N. Fry, Q. Huang, W. B. Dickson, M. H. Dickinson, and X. Deng, "Turning Dynamics and Passive Damping in Flapping Flight," in *Proceedings of 2009 IEEE International Conference on Robotics and Automation*, Kobe, Japan, 2009, pp. 1889-1896.

[6] I. Faruque and J. Sean Humbert, "Dipteran insect flight dynamics. Part 1 Longitudinal motion about hover," *Journal of Theoretical Biology,* vol. 264, pp. 538-552, 2010.

[7] I. Faruque and J. Sean Humbert, "Dipteran insect flight dynamics. Part 2: Lateral-directional motion about hover," *Journal of Theoretical Biology,* vol. 265, pp. 306-313, 2010.

[8] M. Sun and Y. Xiong, "Dynamic flight stability of a hovering bumblebee," *Journal of Experimental Biology,* vol. 208, pp. 447-459, Feb 2005.

[9] Y. Zhang and M. Sun, "Dynamic flight stability of a hovering model insect: lateral motion," *Acta Mechanica Sinica,* vol. 26, pp. 175-190, 2009.

[10] Z. Hu, B. Cheng, and X. Deng, "Lift Generation and Flow Measurements of a Robotic Insect.," in *49th AIAA Aerospace Sciences Meeting*, Orlando, Florida, 2010.

[11] M. H. Dickinson and K. G. Gotz, "Unsteady aerodynamic performance of model wings at low Reynolds number." *Journal of Experimental Biology,* vol. 174, pp. 45-64, 1993

[12] M. H. Dickinson, F. O. Lehmann, and S. P. Sane, "Wing rotation and the aerodynamic basis of insect flight", *Science,* vol. 284, pp. 1954-1960, Jun 1999.

[13] S. P. Sane and M. H. Dickinson, "The aerodynamic effects of wing rotation and a revised quasi-steady model of flapping flight," *Journal of Experimental Biology,* vol. 205, pp. 1087-1096, Apr 2002.